

# Text-guided Image Restoration and Semantic Enhancement for Text-to-Image Person Retrieval

Delong Liu<sup>a</sup>, Haiwen Li<sup>a</sup>, Zhicheng Zhao<sup>a,b,\*</sup>, Yuan Dong<sup>a,b</sup>, Nikolaos V. Boulgouris<sup>c</sup>

<sup>a</sup>*School of Artificial Intelligence, Beijing University of Posts and Telecommunications, Beijing, 100876, China*

<sup>b</sup>*Beijing Key Laboratory of Network System and Network Culture, Beijing, China*

<sup>c</sup>*School of Electronic and Computer Engineering, Brunel University, London, United Kingdom*

---

## Abstract

The goal of Text-to-Image Person Retrieval (TIPR) is to retrieve specific person images according to the given textual descriptions. A primary challenge in this task is bridging the substantial representational gap between visual and textual modalities. The prevailing methods map texts and images into unified embedding space for matching, while the intricate semantic correspondences between texts and images are still not effectively constructed. To address this issue, we propose a novel TIPR framework to build fine-grained interactions and alignment between person images and the corresponding texts. Specifically, via fine-tuning the Contrastive Language-Image Pre-training (CLIP) model, a visual-textual dual encoder is firstly constructed, to preliminarily align the image and text features. Secondly, a Text-guided Image Restoration (TIR) auxiliary task is proposed to map abstract textual entities to specific image regions, improving the alignment

---

\*Corresponding author.

between local textual and visual embeddings. Additionally, a cross-modal triplet loss is presented to handle hard samples, and further enhance the model’s discriminability for minor differences. Moreover, a pruning-based text data augmentation approach is proposed to enhance focus on essential elements in descriptions, thereby avoiding excessive model attention to less significant information. The experimental results show our proposed method outperforms state-of-the-art methods on three popular benchmark datasets, and the code will be made publicly available at <https://github.com/Delong-liu-bupt/SEN>.

*Keywords:*

Text-to-image person retrieval, Cross-modal alignment, Text-guided image restoration, Cross-modal triplet loss

---

## 1. Introduction

Text-to-Image Person Retrieval (TIPR) [36] aims to retrieve person images from a large image gallery based on a given textual description. This task has wide applications in various domains, including social media analysis, image retrieval, and security monitoring. Diverging from conventional text-to-image retrieval [30, 39, 52], TIPR involves searching the target person images from a subjective textual description, which means the queried images have the same category but only differ in some details and attributes. Therefore, it is still an open issue.

Moreover, there exist huge differences in feature representation between visual and textual modalities. The former focuses on conveying information through the intuitive traits, while the latter through vocabulary and gram-

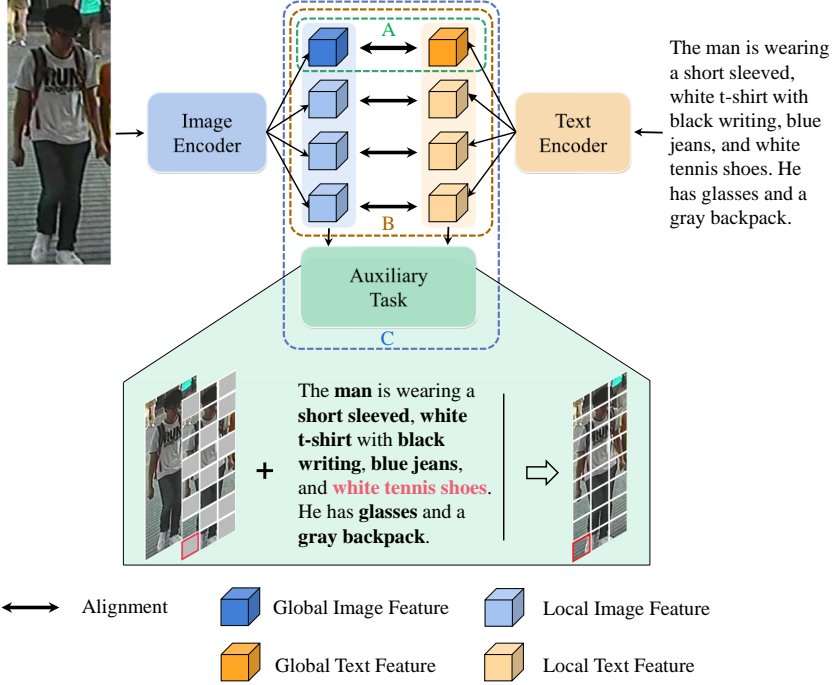


Figure 1: Illustration of the development of text-to-image person retrieval. The green dashed box (A) represents the early global-matching methods where global features are extracted separately from texts and images, followed by a matching and alignment process. The brown dashed box (B) represents subsequent methods that focus on local-matching. These methods explicitly extract local features from both images and texts while performing global and local feature matching and alignment. The blue dashed box (C) indicates more recent approaches that, in addition to feature alignment, leverage joint image-text auxiliary tasks to aid in implicit feature alignment.

mathematical structures, possessing more abstract and flexible characteristics. To address this problem, modal alignment methods are proposed to map visual and textual features into a joint embedding space, thereby facilitating the alignment and matching. Currently, prevalent approaches [13, 19, 60] utilize deep learning to achieve visual and textual feature mapping, and then

compute their similarity for retrieval. These methods can generally be categorized into three types, each focusing on minimizing the feature distance between positively correlated sample pairs.

Early works [19, 43, 65] (Fig. 1A) tend to extract global features separately from images and texts, and use matching losses for modal alignment. Although this kind of approach has the lowest complexity, its performance is generally lower due to the lack of feature interaction. Subsequent methods [10, 54, 64] (Fig. 1B) establish explicit correspondences between local regions in images and phrases in texts, which can significantly improve retrieval performance. However, such methods often require storing feature representations for local regions and phrases and matching them individually, which is inconvenient for large-scale practical scenarios. Recent methods [24, 49, 59] (Fig. 1C) propose to incorporate cooperative auxiliary tasks between visual and textual embeddings on the basis of explicit feature matching, so as to achieve implicit feature alignment. Typical auxiliary tasks include coloring grayscale images according to textual descriptions [59], and recovering randomly masked words in text by images [24]. They appear only in the training phase. Therefore, this type of approach usually does not increase inference complexity, but can achieve higher performance. However, the current auxiliary tasks only focus on specific aspects of visual and textual information rather than establishing thorough semantic correspondences between them. For instance, the coloring task primarily concerns color, while the recovering words task merely emphasizes different masked words in each training iteration.

To tackle these challenges, we introduce a Text-guided Image Restora-

tion (TIR) method aimed at establishing a more robust semantic connection between visual and textual modalities, thereby enhancing the supervision of image-text pair matching. Taking the masked patch marked by the red box as an example (Fig. 1), to effectively restore the missing patch, we generate restoration cues from the image information, and concurrently utilize the phrase “white tennis shoes” to guide the image restoration. Subsequently, fine-grained correspondences between patches in images and phrases in sentences can be implicitly established to enhance the accuracy of text-to-image person retrieval.

Expanding on this foundation, we have developed the cross-modal Semantic Enhancement Network (SEN) to further align textual and visual representations, thereby significantly improving TIPR through enhanced inter-modal coherence. Firstly, to make full use of prior cross-modal alignment knowledge, we build a dual encoder via fine-tuning the CLIP model [42] to obtain the feature representations of image and text. Secondly, a novel auxiliary task TIR, is constructed to maximize the alignment of local visual and textual embeddings. Thirdly, we propose a Cross-Modal Triplet (CMT) loss, which focuses on the most challenging negative samples in a mini-batch to enhance the model’s discriminative ability towards minor differences. Finally, we introduce an innovative text data augmentation technique, which involves selectively omitting less significant vocabulary in sentences, thereby ensuring that the model concentrates on the crucial elements within them. The main contributions of our work can be summarized as follows:

1. To maximize the alignment of visual and textual embeddings, the cross-modal Semantic Enhancement Network (SEN) is introduced, utilizing

a novel text-guided image restoration task to effectively establish correspondences between specific image parts and corresponding textual entities.

2. A cross-modal triplet loss is proposed to force the model to learn the slight differences between hard positive and negative sample pairs, thus the discriminative ability of the model is improved.
3. A novel text data augmentation method that selectively omits non-essential components in sentences, is presented to strengthen model’s ability to identify the key phrases.
4. Extensive experiments show that our SEN outperforms state-of-the-art methods on three public benchmark datasets, i.e., CUHK-PEDES [36], ICFG-PEDES[13], and RSTPReid [66], demonstrating its effectiveness.

## 2. Related work

### 2.1. *Text-to-image Person Retrieval*

As a challenging cross-modal task, TIPR aims to align visual and textual features in a joint embedding space for person matching. There are a series of methods [60, 10, 24], which can be categorized into two main types, i.e., global matching and local matching. Global matching methods [19, 54, 24, 5] primarily focus on learning the overall similarity between images and textual descriptions. Early methods [36, 5, 35] utilize VGG [50] and LSTM [18] to learn representations for images and texts, then align them through matching loss. With the introduction of models like ResNet [20] and Transformer [53], subsequent research improves the backbone networks for feature extraction, such as ResNet50/101 and BERT [12]. In the meantime, new cross-modal

matching loss functions are designed to align global visual and textual features. Local matching methods [60, 10, 54, 46, 56] aim to overcome the limitations of global ones by enhancing local alignment with extra modules [10, 56] or multi-task learning strategies [46, 61], such as human attribute and body pose information. Some methods [10, 46, 61] utilize multi-branch or attention mechanism to learn local features related to body parts, color information, and textual entities to achieve local alignment. These methods outperform those that use global features, but introduce additional computational complexity.

In addition, recent works [24, 49, 59] have explored the utilization of auxiliary tasks to implicitly assist feature alignment. The auxiliary task is utilized only during the network training phase and does not incur additional inference costs, while it enhances network performance. For example, Wu et al. [59] propose the text-guided image coloring as the auxiliary task. Jiang et al. [24] demonstrate the effectiveness of the and Masked Language Modeling [12] (MLM) in person searching.

As for the network initialization, previous methods [49, 16, 34] often initialize parameters with pretrained models from a single modality, which neglects the correspondences between cross-modal information. In recent years, vision-language pretrained models [42, 6, 31, 32, 33] have garnered rising attention. Some works [19, 60] apply the CLIP model to the TIPR task, in which transfer learning is used to transfer CLIP knowledge. The latest research [24] uses the pre-trained CLIP model to TIPR and obtains good performance.

Specifically, our work shares similarities with the [24] only in the use of

CLIP’s pre-trained models as a foundational backbone network, a common practice in our field. Moreover, our approach diverges significantly in several key areas. We have implemented a CMT loss function designed to enhance the network’s ability to discern subtle differences, which is crucial for improving feature discrimination. Additionally, our method incorporates a unique text data augmentation strategy that emphasizes character attributes, effectively complemented by a tailored visual augmentation approach to support our auxiliary tasks. Furthermore, we introduce an auxiliary task involving text-guided image restoration, which demonstrates clear advantages over the auxiliary task used by [24].

## 2.2. *Vision-Language Pre-training*

The “pre-training and fine-tuning” approach [32, 3, 8, 21] has emerged as a critical learning paradigm in deep learning. Vison-language pre-training [42, 32, 11, 63] (VLP) exemplifies this paradigm in cross-modal tasks and has achieved significant advancements. VLP aims to learn the semantic correspondences between visual and textual entities by pre-training on a large-scale dataset [4, 29, 41, 44] of image-text pairs. Inspired by the success of single-modality pre-training methods like BERT[12] and ViT [14], existing works on VLP are mainly based on Transformer [53]. These studies employ a series of elaborately designed pre-training tasks, such as image-text contrastive learning [42, 31, 63], masked language modeling [33, 63]and image caption generation [11, 33], to learn rich and context-aware feature representations with diverse semantic information. These feature representations not only capture the close relationship between visual and textual modalities but also model complex interactions, providing comprehensive cross-modal

representations. Promising results have been achieved on downstream tasks such as image captioning [7], image-text retrieval [28], and visual question answering [1]. VLP models can be divided into single-stream and dual-stream frameworks. Single-stream models [9, 26, 51] consist of a single Transformer encoder, resulting in fewer parameters. In comparison, dual-stream models [42, 15, 23] are well-suited for retrieval tasks. However, they may lack the modeling capacity to capture complex interactions between visual and textual modalities in other vison-language understanding tasks.

Despite some existing challenges, VLP is widely considered a viable approach for large-scale image-text pre-training. In this paper, we further explore how to mine the rich cross-modal knowledge obtained from VLP models and apply it to the TIPR task.

### 3. Method

Our SEN framework is illustrated in Fig. 2. It features dual feature encoders that process both complete and partially masked images, along with a textual input, thereby enriching the feature extraction landscape. A key component, the cross-modal interaction decoder, employs a lightweight design with cross-attention mechanisms, focusing on efficient text-guided image restoration. The architecture is further refined through the integration of four bespoke loss functions (ID [65], SDM [24] , CMT, and MSE loss), each honing in on specific learning objectives such as identity preservation, semantic alignment, and restoration accuracy, crucial for enhancing TIPR performance. Through three representation learning branches and four types of supervision information, the network minimizes the feature distance between

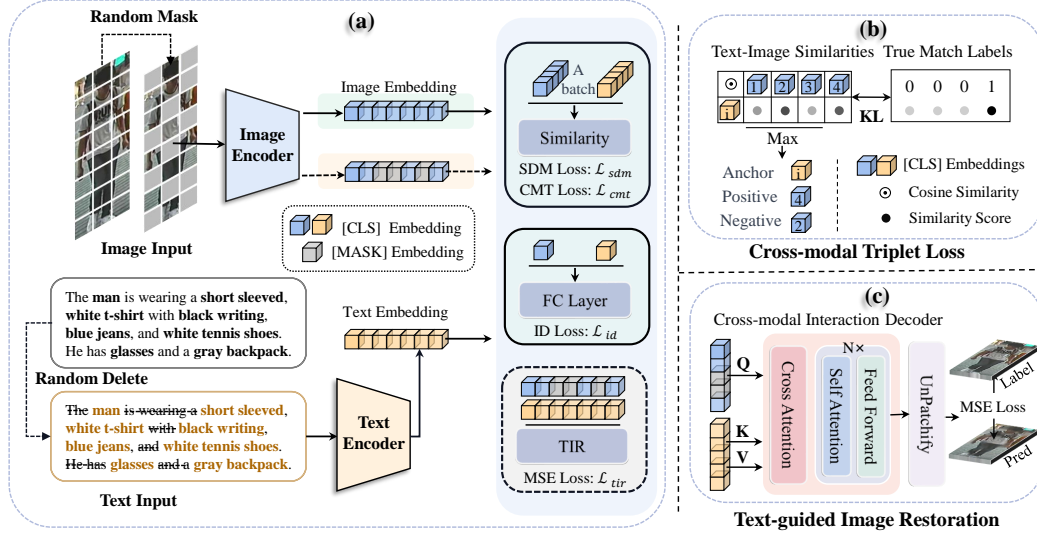


Figure 2: Overview of the proposed SEN framework, which consists of two feature encoders and one cross-modal interaction decoder. (a) SEN utilizes two types of image inputs (complete images and ones with randomly masked patches) and a probability pruning-based text input. The network employs three representation learning branches and four loss functions, including ID loss ( $\mathcal{L}_{id}$ ), SDM loss ( $\mathcal{L}_{sdm}$ ), CMT loss ( $\mathcal{L}_{cmt}$ ), and MSE loss ( $\mathcal{L}_{tir}$ ) in the TIR module. (b) CMT loss compute the loss through selecting the most challenging sample pairs. (c) TIR module uses a lightweight decoder that incorporates cross-attention mechanisms to facilitate efficient text-guided image restoration.

positive pairs in an end-to-end manner. During the inference stage, only the dual-encoder structure is retained, thus the global image-text similarity score is computed only once, resulting in high computational efficiency.

### 3.1. Image Encoder and Text Encoder

The pre-trained full CLIP model is firstly used to initialize the dual encoders in SEN, leveraging the prior knowledge of cross-modal alignment.

### 3.1.1. Image Encoder

Given an input image  $I \in \mathbb{R}^{H \times W \times 3}$ , the pre-trained CLIP ViT model is employed as the image encoder to obtain the embedded representation of the image. Firstly, the image  $I$  is divided into a series of equally-sized and non-overlapping patches, resulting in a total of  $N^v = \frac{H \times W}{P^2}$  patches, where  $P$  represents the size of each patch. Subsequently, these patches are mapped to one-dimensional tokens through a trainable linear projection. To model the global information of these tokens and consider the correlation between patches, an additional [CLS] token is added, to introduce positional information. Next, tokens are input into a model with  $L_v$ -layer Transformer blocks to obtain the feature outputs  $\{f_{\text{cls}}^v, f_1^v, \dots, f_{N^v}^v\}$ , where  $f_{\text{cls}}^v$  represents the global feature, and it is denoted as  $f^v$  in subsequent context.

### 3.1.2. Text Encoder

For the input text  $T$ , the pre-trained CLIP text encoder, is utilized to extract text representations. Firstly, the input text description is tokenized by using the Byte Pair Encoding [45] (BPE) with lowercase. To model the internal correlation of the text, special markers [SOS] and [EOS] are added to the tokenized text sequence to represent the start and end of the sequence, respectively. Additionally, a special marker [CLS] is introduced, and positional information is incorporated into the tokenized text sequence. Next, this sequence of text tokens is input into a  $L_t$ -layer Transformer model, where self-attention mechanism is applied to capture the correlation between each part of the sequence. As a result, we obtain the output of the text encoding:  $\{f_{\text{sos}}^t, f_1^t, \dots, f_{\text{cls}}^t, f_{\text{eos}}^t\}$ , where  $f_{\text{cls}}^t$  represents the global feature, denoted as  $f^t$  in the subsequent context.

### 3.2. Text-guided Image Restoration

As mentioned before, for TIPR, it is very important to establish the correspondences between image and text representations. Therefore, to effectively minimize the pronounced modality gap between vision and language, not only image and text features need to be explicitly aligned, but also a suitable auxiliary task that can assist in achieving fine-grained alignment of image-text features should be considered. Herein, we design a text-guided image restoration module as the auxiliary task to implicitly mine the fine-grained correspondences.

#### 3.2.1. Text-guided Image Restoration

The proposed TIR module aims to maximize the mutual information between images and text by recovering the masked image patches using textual information. We design a lightweight cross-modal decoder and mask a substantial portion of the image to optimize it.

#### 3.2.2. Cross-modal Interaction Decoder

Our cross-modal interaction decoder (Fig. 2(c)) consists of a multi-head cross-attention (MCA) layer and N layers of Transformer blocks, which supervised by maximizing computational efficiency while ensuring sufficient feature interaction.

Given the input image, we first divide the image into a series of equally-sized and non-overlapping image patches. A random masking process is applied to mask a percentage  $p_v$  of the image patches, resulting in a total of  $N_{mask}^v = \lfloor N_p \times p_v \rfloor$  masked patches, which are replaced with a special token [MASK] and are denoted as  $\hat{v}$ , and then are sent to the image encoder

as described in Section 3.1. Then, the final hidden states of the dual encoders  $\{h_i^t\}_{i=1}^L$  and  $\{h_i^{\hat{v}}\}_{i=1}^{N^v}$  are jointly input into the cross-modal interaction encoder, where  $L$  is the length of the input text. To maximize the mutual information between image and text and more effectively fuse textual and masked image representations, the masked image representations  $\{h_i^{\hat{v}}\}_{i=1}^{N^v}$  are used as queries ( $\mathcal{Q}$ ), the textual representations  $\{h_i^t\}_{i=1}^L$  are used as keys ( $\mathcal{K}$ ) and values ( $\mathcal{V}$ ). The global interaction between text and masked image representations can be achieved as follows:

$$\{h_i^c\}_{i=1}^{N^v} = \text{Transformer}(MCA(LN(\mathcal{Q}, \mathcal{K}, \mathcal{V}))) \quad (1)$$

where  $\{h_i^c\}_{i=1}^{N^v}$  represents the context representation of the fused text and masked image,  $LN(\cdot)$  denotes layer normalization, and  $MCA(\cdot)$  represents the multi-head cross-attention, which can be expressed as:

$$MCA(\mathcal{Q}, \mathcal{K}, \mathcal{V}) = \text{softmax}\left(\frac{\mathcal{Q}\mathcal{K}^\top}{\sqrt{d}}\right)\mathcal{V} \quad (2)$$

where  $d$  is the embedding dimension of the masked tokens.

For each masked position  $\{h_i^c\}_{i=1}^{N^v_{mask}}$ , we use a single-layer fully connected network to predict each pixel value within each image patch, denoted as  $Pred$ . Let  $Pred_i^j$  be the value of the  $j$ -th pixel in the  $i$ -th image patch. Consequently, the loss of the TIR module is defined as:

$$\mathcal{L}_{tir} = \frac{1}{N_{mask}^v} \sum_{i=1}^{N_{mask}^v} \sum_{j=1}^{P^2} (Pred_i^j - True_i^j)^2 \quad (3)$$

where  $P$  denotes the size of each image patch, and  $True_i^j$  represents the corresponding ground truth. In contrast to the MLM task, the TIR-based

auxiliary task offers notable advantages when employing a transformer network of the same depth, as it utilizes a significantly lower output dimension in its last fully connected layer, leading to superior performance and efficiency.

### 3.3. Cross-modal Triplet Loss

To further enhance the modeling capability of the model for fine-grained features, a new loss function called Cross-Modal Triplet loss (CMT) is presented. The CMT loss selects the most challenging negative sample pairs from  $B \times B$  image-text pairs for enhanced learning. This approach allows the model to focus on hard samples, thereby improving its encoding ability of capturing subtle differences.

Given a mini-batch of data containing  $B$  image-text pairs, we construct a set of image-text pairs  $\{(f_i^v, f_j^t), y_{i,j}\}_{j=1}^B$  for the global representation  $f_i^v$  of each image, where  $y_{i,j}$  is a binary label indicating whether  $(f_i^v, f_j^t)$  belongs to the same identity ( $y_{i,j} = 1$ ) or not ( $y_{i,j} = 0$ ). Let  $\text{sim}(\mathbf{u}, \mathbf{v}) = \mathbf{u}^\top \mathbf{v} / \|\mathbf{u}\| \|\mathbf{v}\|$  be the cosine similarity. The probability of a correct match can be calculated based on the softmax function as follows:

$$p_{i,j} = \frac{\exp(\text{sim}(f_i^v, f_j^t) / \tau)}{\sum_{k=1}^B \exp(\text{sim}(f_i^v, f_k^t) / \tau)} \quad (4)$$

where  $\tau$  is a temperature hyperparameter that controls the peakiness of the probability distribution. The matching probability  $p_{i,j}$  can be seen as the proportion of the similarity score between  $f_i^v$  and  $f_j^t$  and the sum of cosine similarity scores between  $f_i^v$  and  $\{f_j^t\}_{j=1}^B$  in the mini-batch. For each image representation  $f_i^v$ , the weakest positive sample  $p_i^t = \min \{f_j^t, y_{i,j} = 1\}_{j=1}^B$  and the hardest negative sample  $n_i^t = \max \{f_j^t, y_{i,j} = 0\}_{j=1}^B$  can be chosen in the mini-batch. Accordingly, the CMT loss from image to text in each mini-batch

is calculated as:

$$\mathcal{L}_{i2t} = \frac{1}{B} \sum_{i=1}^B [\text{sim}(f_i^v, p_i^t) - \text{sim}(f_i^v, n_i^t) + \alpha]_+ \quad (5)$$

where  $\text{sim}(\cdot, \cdot)$  denotes the cosine similarity,  $\alpha$  is a hyperparameter, and  $[x]_+$  denotes the positive value operation, i.e.,  $[x]_+ = \max(0, x)$ .

Similarly, the CMT loss  $\mathcal{L}_{t2i}$  from text to image can be obtained by exchanging  $f^v$  and  $f^t$  in the above formulas. The bidirectional CMT loss is computed as:

$$\mathcal{L}_{cmt} = \mathcal{L}_{i2t} + \mathcal{L}_{t2i} \quad (6)$$

To further improve the learning of global representations for images and text in the joint embedding space, we also combine an ID loss [65] and an SDM [24] loss. The ID loss ( $\mathcal{L}_{id}$ ) is a classification loss, which used to categorize the embedding vectors of images or text into different identity classes for supervised training. By introducing the ID loss, the feature representations belonging to the same identity within the same modality can be brought closer, thus promoting the alignment of features between images and texts. The SDM loss utilizes KL divergence to simultaneously supervise the embedding of image-text pairs in the same mini-batch, aiming to decrease the distance between positive pairs and increase the distance between negative pairs in the joint embedding space, thereby associating the feature representations of different modalities.

In conclusion, SEN is trained in an end-to-end manner, with the overall optimization objective defined as:

$$\mathcal{L} = \mathcal{L}_{tir} + \mathcal{L}_{cmt} + \mathcal{L}_{sdm} + \mathcal{L}_{id} \quad (7)$$

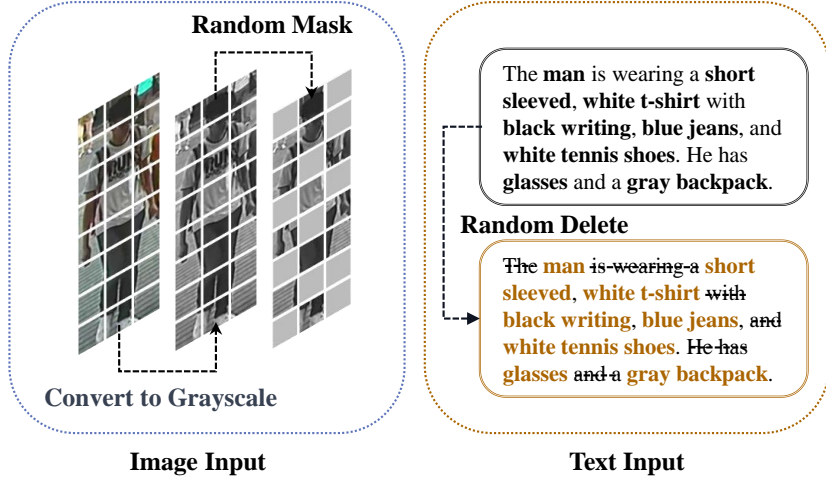


Figure 3: Illustration of data augmentation methods for the visual and textual modalities. The blue box on the left represents the conversion of image input to grayscale during the execution of the TIR auxiliary task. The grayscale image is then randomly masked and fed into the network, which is still required to recover the color image. The brown box on the right represents the deletion of non-key parts in sentences with a certain probability for text input.

### 3.4. Data Augmentation

Attributes such as color and texture play a crucial role in person retrieval [37, 40, 55]. Hence, revolving around this key aspect, we design novel data augmentation method for the visual and textual modalities.

#### 3.4.1. Text Data Augmentation Based on Attribution

For the text modality, it is desired that the network is able to recognize and emphasize the key components relevant to person retrieval in the sentences. Therefore, it is important to establish an effective cueing mechanism and enable the network to quickly capture these crucial pieces of information. For text inputs, we propose using the NLTK library [2] to perform

part-of-speech tagging, assigning a small probability to selectively preserve words identified as pronouns, adjectives, nouns, and certain verbs intermixed among them. Following this filtering, the network is then trained using these modified sentences. This approach guides the network to rely more on the attribute information in the sentences for subsequent supervised tasks. Consequently, when processing complete sentences, the network prioritizes the use of attribute information, thereby enhancing the efficiency of person retrieval. Additionally, this method also enhances the robustness of the approach to different linguistic styles of sentences.

#### *3.4.2. Visual Data Augmentation*

Similar to the enhancement mechanism of text modality, in visual modality, it is also crucial to increase the implicit alignment between color-related vocabulary in the textual modality and certain image regions. Inspired by [59], we process the images by converting them to grayscale, and subsequently task the network with restoring the original color images. After employing data augmentation, all image blocks that are not masked will no longer carry color information. Consequently, the restoration of full-color images necessitates the capture of color information from the text, thereby increasing the model’s reliance on the color information present in the text. This treatment guides more attention to the color information, which is critical for implicit alignment of text phrases and image regions, improving auxiliary supervision.

## **4. Experiments**

Three challenging text-to-image person retrieval datasets are employed, and comprehensive evaluations are conducted. Comparisons are made against

Method	Type	Image Encoder	Text Encoder	Rank-1	Rank-5	Rank-10	mAP	mINP
CMPM/C[64] [ECCV18]	L	RN50	LSTM	49.37	-	79.27	-	-
PMA[25] [AAAI20]	L	RN50	LSTM	53.81	73.54	81.23	-	-
TIMAM[43] [ICCV'19]	G	RN101	BERT	54.51	77.56	79.27	-	-
ViTAA[54] [ECCV20]	L	RN50	LSTM	54.92	75.18	82.90	51.60	-
NAFS[17] [arXiv21]	L	RN50	BERT	59.36	79.13	86.00	54.07	-
DSSL[66] [MM21]	L	RN50	BERT	59.98	80.41	87.56	-	-
SSAN[13] [arXiv21]	L	RN50	LSTM	61.37	80.15	86.73	-	-
LapsCore[59] [ICCV21]	L	RN50	BERT	63.40	-	87.80	-	-
ISANet[61] [arXiv22]	L	RN50	LSTM	63.92	82.15	87.69	-	-
LBUL[57] [MM22]	L	RN50	BERT	64.04	82.66	87.22	-	-
CM-MoCo[19] [BMVC21]	G	CLIP-RN101	CLIP-Xformer	64.08	81.73	88.19	60.08	-
SAF[34] [ICASSP22]	L	ViT-Base	BERT	64.13	82.62	88.40	-	-
TIPCB[10] [Neuro22]	L	RN50	BERT	64.26	83.19	89.10	-	-
CAIBC[56] [MM22]	L	RN50	BERT	64.43	82.87	88.37	-	-
AXM-Net[16] [MM22]	L	RN50	BERT	64.44	80.52	86.77	58.73	-
PBSL [48] [MM23]	L	RN50	BERT	65.32	83.81	89.26	-	-
BEAT [38] [MM23]	L	RN101	BERT	65.61	83.45	89.57	-	-
LGUR[46] [MM22]	L	DeiT-Small	BERT	65.25	83.12	89.00	-	-
IVT[49] [ECCVW22]	G	ViT-Base	BERT	65.59	83.11	89.21	-	-
UniPT[47] [ICCV23]	G	CLIP-ViT-B/16	CLIP-Xformer	68.50	84.67	90.38	-	-
Gen [58] [TCSVT23]	G	ViT-Base	BERT	69.47	87.13	92.13	60.56	-
CFine[60] [arXiv22]	L	CLIP-ViT-B/16	BERT	69.57	85.93	91.15	-	-
IRRA[24] [CVPR23]	G	CLIP-ViT-B/16	CLIP-Xformer	73.38	89.93	93.71	66.13	50.24
<b>Baseline</b>	G	CLIP-ViT-B/16	CLIP-Xformer	71.23	87.80	92.59	65.02	49.21
<b>SEN(ours)</b>	G	CLIP-ViT-B/16	CLIP-Xformer	<u>75.00</u>	<u>89.98</u>	<u>94.09</u>	<u>67.23</u>	<u>51.45</u>
<b>SEN-XL(ours)</b>	G	CLIP-ViT-L/14	CLIP-Xformer	<b>76.64</b>	<b>91.33</b>	<b>94.66</b>	<b>69.19</b>	<b>53.88</b>

Table 1: Comparison with state-of-the-art methods on the CUHK-PEDES dataset. In the “Type” column, “G” and “L” represent global matching and local matching methods, respectively.

state-of-the-art methods. Meanwhile, the effectiveness of each component in our proposed framework is demonstrated through rigorous ablation study.

#### 4.1. Datasets and Evaluation Metrics

**The CUHK-PEDES dataset** [36] is the first dataset dedicated to text-to-image person retrieval, comprising 40,206 images and 80,412 text descriptions, covering 13,003 identities. The training set consists of 34,054 images and 68,108 text descriptions, while the validation and test sets contain 3,078 and 3,074 images, respectively, each accompanied by 6,158 and 6,156 text descriptions. Both the validation and test sets include 1,000 identities. These images have been manually annotated, with each image having two descriptions, and the average length of all the descriptions is no less than 23 words.

**The ICFG-PEDES dataset** [13] consists of 54,522 images and their corresponding text descriptions, covering 4,102 identities. Each image has only one corresponding text description. The dataset is divided into a training set and a test set, with the training set containing 34,674 image-text pairs, covering 3,102 identities, and the test set containing 19,848 image-text pairs, covering 1,000 identities. Compared to CUHK-PEDES, ICFG-PEDES places more emphasis on individual identities and provides more finer-grained information in the textual descriptions. The average length of the descriptions is 37 words, and the vocabulary contains 5,554 different words.

**The RSTPReid dataset** [66] comprises 20,505 images and 41,010 text descriptions, covering 4,101 identities. Each identity has 5 images, and each image corresponds to 2 text descriptions, with each description having a minimum length of 23 words. The dataset is captured by 15 cameras and is designed to address text-to-image person retrieval tasks in real-world scenarios. It is divided into a training set (3,701 identities), a validation set (200 identities), and a test set (200 identities).

The popular Rank-k metric is used to evaluate the performance. This metric measures the probability of finding at least one matching person image within the top k candidates given a text query. Common values for k are 1, 5, and 10. A higher Rank-k score indicates that the system is more effective in returning relevant results for the query. In addition to using the mean average precision (mAP) for evaluation, the mean Inverse Negative Penalty [62] (mINP) is introduced as an additional evaluation criterion. The mAP considers the model’s performance on different queries by calculating the average precision of retrieved relevant images and averaging the results across all queries, while mINP combines the ranking and relevance of image-text retrieval by calculating the inverse negative penalty for relevant image-text pairs and averaging the results across all queries. Higher values of Rank-k, mAP, and mINP indicate superior performance.

#### *4.2. Implementation Details*

We perform our experiments on a single A100 80GB GPU. The image encoder and text encoder are initialized with pre-trained CLIP parameters, while the parameters of the TIR module are randomly initialized. For each layer of the TIR module’s decoder, the hidden feature size and the number of heads are set to 512 and 8, respectively. During the training process, in addition to the data augmentation method mentioned in section 3.4, we apply random horizontal flipping, random cropping with padding, and random erasing to the image data. The input images are resized to  $384 \times 128$ , with each patch size being  $16 \times 16$ . The maximum length of the textual token sequence is set to 77, and there is a 0.2 probability of retaining keywords. We utilize the Adam [27] optimizer for training, performing a total of 60 epochs

with an initial learning rate of  $10^{-5}$ . We employ cosine learning rate decay. Initially, we conduct 5 warm-up epochs, gradually increasing the learning rate from  $10^{-6}$  linearly to  $10^{-5}$ . For the randomly initialized modules, the initial learning rate is set to  $5 \times 10^{-5}$ . The temperature parameter  $\tau$  in both the CMT and SDM loss is set to 0.02. During training, the entire SEN model is trained, while during testing, only the dual-encoder structure is retained.

#### 4.3. Comparisons with State-of-the-art Models

In this section, we present our baseline, which is the pre-trained CLIP model fine-tuned with loss SDM [24] and loss ID [65]. We compare our method with state-of-the-art approaches on three benchmark datasets as shown in Tables 1, 2, and 3. Our method demonstrates significant improvements over the baseline on all three benchmark tests and achieves the best results.

**Evaluatuion on the CUHK-PEDES:** Firstly, we evaluate our SEN model on this dataset. From the results in Table 1, it can be observed that SEN achieves Rank-1, Rank-5, and Rank-10 accuracies of 75.00%, 89.98%, and 94.08% respectively, with a mAP of 67.23%. Compared to recent state-of-the-art methods, SEN demonstrates superior performance. Additionally, we note that recent advanced methods tend to utilize Transformer structures for image-text feature extraction. Furthermore, the performance of our baseline model indicates that fine-tuning the pre-trained full CLIP model is a good choice. Compared to the baseline, our method achieves a 3.73% improvement in Rank-1 accuracy and a 2.21% improvement in mAP. Compared to IRRA[24], which fine-tunes the entire CLIP as well, our method exhibits significant advantages across all evaluation metrics. Furthermore, SEN-XL

Method	Type	Rank-1	Rank-5	Rank-10	mAP	mINP
Dual Path[65] [TOMM20]	G	38.99	59.44	68.41	-	-
CMPM/C[64] [ECCV18]	L	43.51	65.44	74.26	-	-
ViTAA[54] [ECCV20]	L	50.98	68.79	75.78	-	-
SSAN[13] [arXiv21]	L	54.23	72.63	79.53	-	-
TIPCB[10] [Neuro22]	L	54.96	74.72	81.89	-	-
IVT[49] [ECCVW22]	G	56.04	73.60	80.22	-	-
Gen [58] [TCSVT23]	G	57.69	75.79	82.67	36.07	-
ISANet[61] [arXiv22]	L	57.73	75.42	81.72	-	-
PBSL [48] [MM23]	L	57.84	75.46	82.15	-	-
BEAT [38] [MM23]	L	58.25	75.92	81.96	-	-
UniPT[47] [ICCV23]	G	60.09	76.19	82.46	-	-
CFine[60] [arXiv22]	L	60.83	76.55	82.42	-	-
IRRA[24] [CVPR23]	G	63.46	80.25	85.82	38.06	7.93
<b>Baseline(ViT-B)</b>	G	61.07	78.32	83.91	35.96	7.14
<b>SEN(ViT-B)</b>	G	<u>64.56</u>	<u>80.49</u>	<u>85.88</u>	<u>40.80</u>	<u>9.51</u>
<b>SEN-XL(ViT-L)</b>	G	<b>66.76</b>	<b>81.57</b>	<b>86.55</b>	<b>44.28</b>	<b>12.26</b>

Table 2: Comparison with state-of-the-art methods on the ICFG-PEDES dataset.

demonstrates that our method yields substantial performance improvements when using larger models.

**Evaluatuion on the ICFG-PEDES:** The performance comparison on the ICFG-PEDES dataset is shown in Table 2. The baseline method achieves Rank-1, Rank-5, and Rank-10 accuracies of 61.07%, 78.32%, and 83.91% respectively. This result demonstrates the strong performance of directly fine-tuning the pre-trained full CLIP model on this task, with performance

Method	Type	Rank-1	Rank-5	Rank-10	mAP	mINP
DSSL[66] <small>[MM21]</small>	G	39.05	62.60	73.95	-	-
SSAN[13] <small>[arXiv21]</small>	L	43.50	67.80	77.15	-	-
LBUL[57] <small>[MM22]</small>	L	45.55	68.20	77.85	-	-
IVT[49] <small>[ECCVW22]</small>	L	46.70	70.00	78.80	-	-
PBSL [48] <small>[MM23]</small>	L	47.78	71.40	79.90	-	-
BEAT [38] <small>[MM23]</small>	L	58.25	73.10	81.30	-	-
CFine[60] <small>[arXiv22]</small>	L	50.55	72.50	81.60	-	-
UniPT[47] <small>[ICCV23]</small>	G	51.85	74.85	82.85	-	-
IRRA[24] <small>[CVPR23]</small>	G	60.20	81.30	<u>88.20</u>	47.17	25.28
<b>Baseline(ViT-B)</b>	G	58.65	80.70	87.10	46.54	24.02
<b>SEN(Ours)</b>	G	<u>61.60</u>	<u>81.75</u>	88.05	<u>48.62</u>	<u>26.43</u>
<b>SEN-XL(ViT-L)</b>	G	<b>62.70</b>	<b>83.60</b>	<b>89.15</b>	<b>49.89</b>	<b>27.56</b>

Table 3: Comparison with state-of-the-art methods on the RSTPReid dataset

slightly lower than the IRRA. Compared to the baseline, our method improves Rank-1 accuracy by 3.49% and mAP by 4.84%. Compared to [24], our method achieves a 1.10% improvement in Rank-1 accuracy and a 2.74% improvement in mAP, establishing a leading advantage across all evaluation metrics. Furthermore, SEN-XL significantly outperforms all existing methods. Note that the mINP metric on the ICFG-PEDES dataset is generally low, indicating the difficulty of fully identifying all person images of an identity within this dataset.

**Evaluatuion on the RSTPReid:** The comparison results on the RSTPReid dataset are shown in Table 3. SEN-XL continues to achieve the best performance. Our method achieves a 2.95% improvement in Rank-1 accu-

racy and a 2.08% improvement in mAP compared to the baseline. Compared to [24], our method achieves a gain of 1.40% in Rank-1 accuracy and 1.45% in mAP, and significantly outperforms other methods. SEN-XL consistently delivers superior performance.

In conclusion, SEN consistently achieves the best performance on all three popular benchmark datasets. This demonstrates the generalization capability and robustness of our proposed method.

#### *4.4. Computational Efficiency of SEN*

The SEN achieves high computational efficiency during inference, as it does not require multi-stage matching or localized matching procedures. Our performance evaluations were conducted on an Intel(R) Xeon(R) Platinum 8358P CPU @ 2.60GHz with a single A100 GPU. Specifically, the inference tests utilized the test sets of all three popular datasets in this domain, comprising 28,004 text entries and 23,922 image entries. The bulk of the time was dedicated to feature extraction, taking 6.44 seconds for texts and 29.91 seconds for images. Calculating similarities through matrix operations was completed in merely 9 ms.

In practical application scenarios, such as an initial retrieval from a database containing 20,000 images for every 1,000 text entries, the time required was 25.24 seconds. Subsequent searches for each additional set of 1,000 texts, where image features did not need to be re-extracted, took only 0.23 seconds. For real-time monitoring scenarios—assuming a scenario where each frame contains approximately 100 individuals with 10 texts requiring queries—our framework managed to process 7.85 frames per second, satisfying real-time retrieval requirements. For users demanding superior perfor-

No.	Components		CUHK-PEDES			ICFG-PEDES		
	Vision	Text	Rank-1	Rank-5	Rank-10	Rank-1	Rank-5	Rank-10
1			74.76	89.69	93.81	64.32	80.32	85.64
2	✓		74.85	89.77	93.82	64.4	80.41	85.67
3		✓	74.91	89.82	94.00	64.49	80.43	85.79
4	✓	✓	<b>75.00</b>	<b>89.98</b>	<b>94.08</b>	<b>64.56</b>	<b>80.49</b>	<b>85.88</b>

Table 4: Ablation experimental results with different data augmentation techniques. “Vision” represents image-side data augmentation, “Text” represents text-side data augmentation, and “✓” indicates the usage of a particular augmentation technique.

mance, the extended version of the model, SEN-XL, can be employed, albeit at a 41% reduction in efficiency compared to the standard model. This allows users to balance between efficiency and performance based on specific needs.

#### 4.5. Ablation Study

In order to thoroughly demonstrate the effectiveness of each component, we conduct extensive ablation experiments where the pre-trained full CLIP model fine-tuned with SDM loss and ID loss is used as the baseline.

##### 4.5.1. The Effectiveness of Data Augmentation

To validate the impact of the proposed two data augmentation techniques, we perform related ablation experiments on CUHK-PEDES and ICFG-PEDES, and the results under different experimental settings are recorded in Table 4. The effectiveness of visual data augmentation is orderly demonstrated by comparing the results from (No.1 to No.2) and (No.3 to No.4). The effectiveness of text data augmentation is verified by comparing (No.1 to No.3) and (No.2 to No.4). Using each data augmentation individually can bring

performance improvement to some extent, but the best results are achieved when both data augmentation techniques are used together.

Specially, in order to validate the effectiveness of our visual data augmentation method in enhancing color information, we conducted a specific experiment using the CUHK-PEDES test set. Specifically, we calculated the average reduction in cosine similarity between sentences from which all color-related words were removed and their corresponding images, compared to the original sentences. Similarly, we computed the average reduction in cosine similarity for sentences from which individual color words were randomly removed. Without the use of visual data augmentation, the average decrease in cosine similarity for the removal of all color words was 0.0703, and for the removal of individual color words, it was 0.0153. However, with the implementation of visual data augmentation, these values changed to 0.0813 and 0.0170, respectively. This shift demonstrates that our method significantly directs the model’s attention more toward color information.

#### *4.5.2. The Effectiveness of Proposed Components*

In order to thoroughly demonstrate the impact of different components in SEN, we conduct comprehensive experiments on CUHK-PEDES and ICFG-PEDES. The Rank-1, Rank-5, and Rank-10 accuracies (%) under different experimental settings are recorded in Table 5. Results show the positive role of our proposed each component. These results also indicate that adding additional supervised loss ( $\mathcal{L}_{cmt}$ ) for hard samples can lead to performance improvement.

Specifically, the TIR module facilitates fine-grained cross-modal alignment by implicitly learning the local correspondences between image patches

No.	Methods	Components			CUHK-PEDES			ICFG-PEDES		
		CMT	IRR	TIR	Rank-1	Rank-5	Rank-10	Rank-1	Rank-5	Rank-10
1	Baseline				71.23	87.80	92.59	61.07	78.32	83.91
2	$\mathcal{L}_{cmt}$	✓			71.62	87.93	92.71	61.32	78.46	84.09
3	IRR		✓		73.40	89.59	93.72	63.49	80.31	85.81
4	TIR			✓	74.71	89.73	93.89	64.27	80.33	85.85
5	$\mathcal{L}_{cmt}$ +IRR	✓	✓		73.84	89.85	93.81	63.76	80.31	85.84
6	IRR+TIR		✓	✓	74.45	89.67	93.74	64.09	80.28	85.79
7	$\mathcal{L}_{cmt}$ +IRR+TIR	✓	✓	✓	74.62	89.78	93.84	64.26	80.38	85.85
8	<b>SEN</b>	✓		✓	<b>75.00</b>	<b>89.98</b>	<b>94.08</b>	<b>64.56</b>	<b>80.49</b>	<b>85.88</b>

Table 5: Ablation experimental results on the effectiveness of each component in SEN(ViT-B). The “Baseline” represents the pre-trained full CLIP model fine-tuned with SDM loss and ID loss. Subsequent experimental settings utilize these two loss functions and the best data augmentation strategy.

and text phrases through the Masked Image Modeling (MIM) [22] task. When only the TIR module is added to the baseline, the Rank-1 accuracies on both datasets are improved by 3.28% and 3.13%, respectively. Compared with the proven effective IRR [24] auxiliary task, our TIR maintains advantages of 1.31% and 0.78% in Rank-1 accuracy on the two datasets.

It is worth noting that the comparisons from two groups that is, No.4 with No.6, and No.7 with No.8, indicate that integrating two effective auxiliary tasks simultaneously does not necessarily lead to better results. In fact, it may even result in lower training efficiency and poorer performance.

#### 4.5.3. Ablation Experiments on the TIR Module

To maximize the efficiency of our proposed cross-modal interaction module, we explore the influence of the depth of it and the image masking ratio. The variations in Rank-1 accuracy and mAP under different depths of the

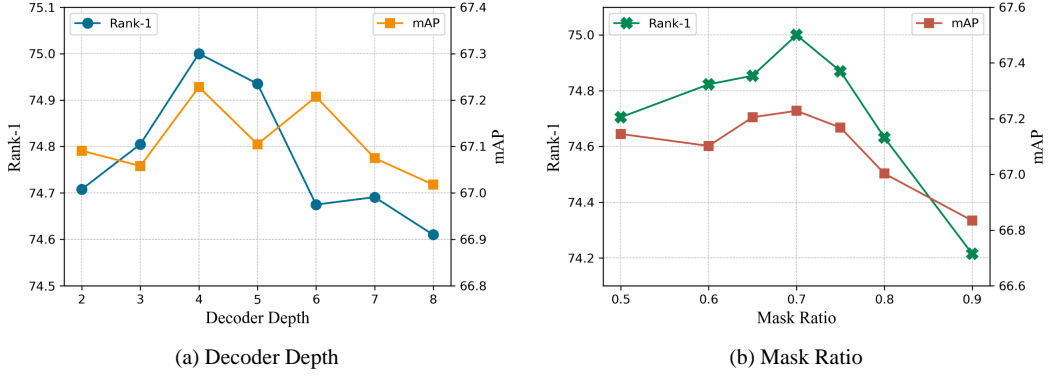


Figure 4: Ablation experiment results of the TIR module. (a) illustrates the Rank-1 and mAP metrics of SEN under different depths of the cross-modal interaction decoder. (b) demonstrates the Rank-1 and mAP metrics of SEN input with varying image masking ratios when utilizing the TIR module.

cross-modal interaction decoder are shown in Fig. 4(a). It is evident that a depth of 4 is the optimal choice. Additionally, Fig. 4(b) shows that an image masking ratio of 0.7 is the best choice, as a very high image masking ratio (e.g., 0.9) would produce negative impact.

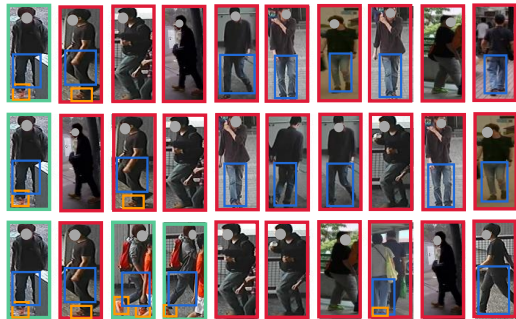
#### 4.6. Qualitative Results

Fig. 5 compares the top-10 retrieval results with the baseline, [24], and our proposed SEN. It is evident that SEN achieves more accurate retrieval results and demonstrates heightened sensitivity to descriptions of the same identity. In most cases, even with variations in viewpoint, SEN is able to find all targets of the same identity within the top-10 retrieval results. In contrast, both the baseline and IRRA methods do not exhibit this advantageous characteristic. The reason for this improvement can be attributed to two factors. Firstly, the TIR module helps to establish the correlations between text phrases and local image regions, thereby reducing the over-reliance on

The man is wearing a **striped collared shirt**. He is wearing black pants and black shoes. He carries a **book** and his **black coat** in his **left hand**.



A man wearing a black shirt, a pair of **blue jeans** and a pair of **orange shoes**.



The lady is wearing a **red mid sleeve shirt** tucked into a **light blue ruffled skirt** with **blue heels** and a **blue purse with white handles** on her right shoulder.



Figure 5: Comparison of the top 10 retrieval results between the baseline (first row), IRRA [24] (second row), and SEN (third row) on CUHK-PEDES. Matching and non-matching images corresponding to the text description are highlighted with green and red bounding boxes, respectively. The matched textual entities and local image regions are indicated with phrases and bounding boxes of the same color in the figure.

visual perspectives in person retrieval. Secondly, the CMT loss focuses more on challenging person cases and enables the network to differentiate subtle

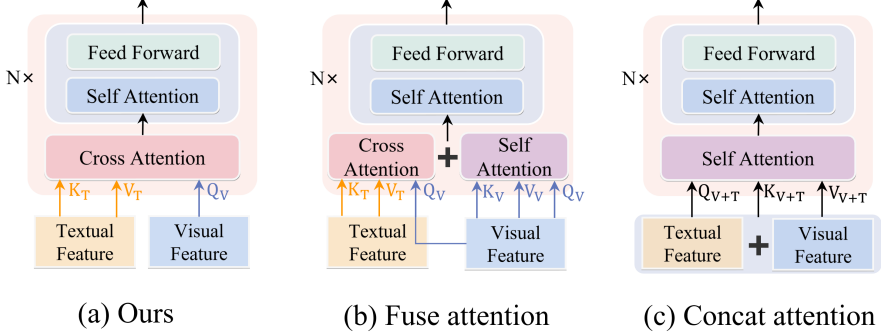


Figure 6: Illustration of different cross-modal interaction decoders. (a) Our cross-modal interaction encoder, where visual information is used as the query, and textual information serves as key and value for cross attention before being fed into the Transformer Block. (b) Fuse attention, where visual information is used as the query, and both visual and textual information are used as key and value for separate attention before being combined and fed into the Transformer Block. (c) Concat attention, where visual and textual information are concatenated for self-attention before being fed into the Transformer Block.

differences between different identities. Furthermore, the correspondences between text phrases and image patches in the figure also indicate that SEN has stronger local alignment capability. Taking the first group of images in Fig. 5 as an example, the sentence contains the phrase “black coat in his left hand,” and SEN finds the corresponding images in the top three retrieval results, rather than focusing separately on “black coat” and “hand.”

## 5. Discussion

### 5.1. How Auxiliary Tasks Enhance Retrieval Performance

Currently, incorporating an auxiliary task into the text-to-image person retrieval framework has become a promising practice. However, when choosing auxiliary task, a question arises: does better performance in an auxiliary

Method	Rank-1	Rank-5	Rank-10
Fuse attention	74.76	89.86	93.97
Concat attention	74.69	89.80	94.01
<b>Ours</b>	<b>75.00</b>	<b>89.98</b>	<b>94.08</b>

Table 6: Performance table of SEN using different cross-modal interaction decoders.

task guarantee better final retrieval results? This section aims to answer this question by evaluating TIR module with different cross-modal attention mechanisms.

As shown in Fig. 6, we evaluated three distinct cross-modal interaction decoders by integrating them into the complete network for training and testing on the CUHK-PEDES dataset. Fig. 7 presents the visualization results of the TIR, and Table 6 shows the final retrieval performance. Upon comparing the image restoration results from the three different cross-modal interaction decoders in Fig. 7, it becomes evident that the ‘fuse attention’ and ‘concat attention’ methods yield superior image restoration. However, the test results in Table 6 indicate that using our cross-modal interaction encoder achieves the best retrieval performance. The reason for this could be attributed to the different cross-modal interaction methods in Fig. 6(b) and Fig. 6(c). In the image restoration process, the visual information is not only used as the query but is also directly involved in the restoration. Although this contributes to better image restoration, it significantly weakens the dependency of the auxiliary task on text and hampers the interaction between images and texts. In contrast, our approach uses visual information as the query and textual information as key and value, forcing the network to utilize

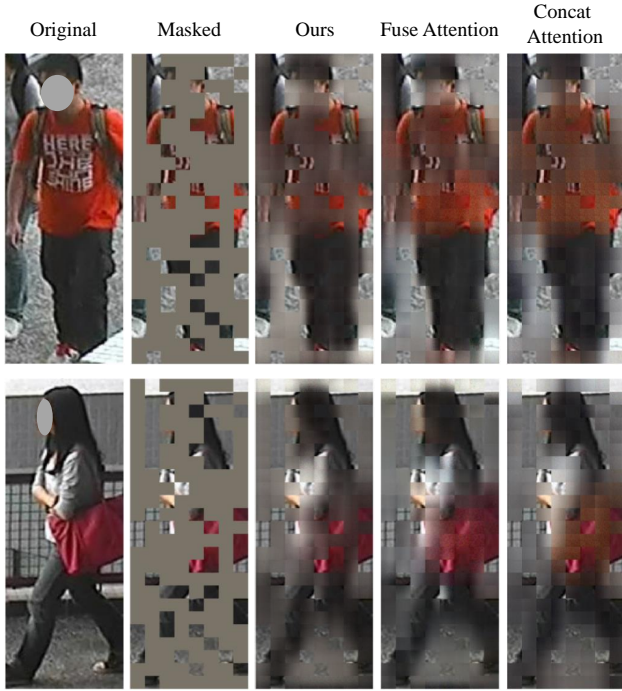


Figure 7: Illustration of image restoration results using different cross-modal interaction decoders. For each set of images, from left to right, they represent the original image, the image after being masked, and the images restored by three forms of cross-attention in the cross-modal interaction decoders (from left to right: Ours, Fuse attention, and Concat attention). The auxiliary task is aimed at enhancing retrieval, not at achieving excellence in the task itself. Hence, we have not provided extra supervision or optimization to the image restoration function, resulting in its modest visual quality.

textual information to recover the masked image patches through cross-modal attention. Although this is a challenging task, it significantly increases the demand for interaction between texts and images, thereby achieving better retrieval performance.

In summary, pursuing better performance in auxiliary task can not guarantee better performance in text-to-image person retrieval. The key to im-

proving retrieval performance lies in enhancing the interaction and connection between texts and images. By reinforcing the relationship between textual and visual entities, we ultimately achieve better results.

### 5.2. Robustness of the Methods

Method	Domin	R1	R5	mAP	Domin	R1	R5	mAP
<b>IRRA</b> w/o IRR	CUHK → RSTP	53.30 -0.20↓	77.15 -0.05↓	39.63 -0.09↓	CUHK → ICFG	42.42 -0.38↓	62.11 -0.15↓	21.77 -0.16↓
<b>IRRA</b> w/o IRR	ICFG → RSTP	45.30 -0.10↓	69.35 +0.05↑	36.83 -0.04↓	ICFG → CUHK	33.46 -0.44↓	56.30 -0.21↓	31.56 -0.23↓
<b>IRRA</b> w/o IRR	RSTP → ICFG	32.30 -0.33↓	49.69 -0.20↓	20.54 -0.19↓	RSTP → CUHK	32.80 -0.32↓	55.25 -0.11↓	30.29 -0.19↓
<b>SEN</b> w/o Augt w/o TIR w/o $\mathcal{L}_{cmt}$	CUHK → RSTP	55.50 -1.35↓ -0.95↓ -0.20↓	77.85 -0.75↓ -0.70↓ +0.05↑	45.29 -1.07↓ -0.64↓ -0.14↓	CUHK → ICFG	45.34 -1.81↓ -1.57↓ -0.47↓	63.45 -1.01↓ -0.95↓ -0.10↓	23.26 -0.98↓ -0.73↓ -0.31↓
<b>SEN</b> w/o Augt w/o TIR w/o $\mathcal{L}_{cmt}$	ICFG → RSTP	47.45 -1.05↓ -1.00↓ +0.05↑	71.95 -0.65↓ -0.55↓ -0.20↓	39.86 -0.98↓ -0.81↓ -0.09↓	ICFG → CUHK	37.88 -2.01↓ -1.72↓ -0.47↓	60.48 -1.33↓ -0.93↓ -0.31↓	35.07 -1.44↓ -1.07↓ -0.35↓
<b>SEN</b> w/o Augt w/o TIR w/o $\mathcal{L}_{cmt}$	RSTP → ICFG	36.23 -1.99↓ -1.56↓ -0.39↓	53.31 -1.52↓ -1.12↓ -0.21↓	22.32 -1.56↓ -1.12↓ -0.30↓	RSTP → CUHK	35.40 -1.57↓ -0.89↓ -0.42↓	57.71 -1.12↓ -0.49↓ -0.25↓	33.41 -1.09↓ -0.74↓ -0.37↓

Table 7: Performance of methods and components in cross-domain tests. w/o in the table indicates the performance of the original method with the corresponding component removed.  $Aug_t$  represents text-side data augmentation. Performance increases are marked in red, and decreases in blue. CUHK-PEDES is abbreviated as CUHK, ICFG-PEDES as ICFG, and RSTPReid as RSTP. The arrow → indicates that the method was trained on the dataset on the left and tested on the dataset on the right.

The robustness of a method is crucial for its applicability in real-world scenarios. To this end, we conducted cross-domin tests on all popular datasets and compared them with existing high-performance method. To clearly observe the impact of our designed components on the robustness of the method, we also conducted control experiments by removing components from the method, with results shown in Table 7.

From the results in the table, it is evident that every method suffers some performance loss in the face of cross-domin testing, due to differences in image sources and annotation styles across datasets. However, regardless of how the cross-domain tests were conducted, the SEN method consistently achieved the best performance. By examining the performance changes resulting from the removal of key components, we found that highlighting person attributes that are invariant to language style changes effectively improves the method’s robustness. Specifically, when text data augmentation in the SEN method was removed, it had the most significant impact on cross-domain testing indicators. Our text data augmentation method emphasizes key attributes in text, which, although it showed only minor effectiveness in experiments trained and tested on the same dataset (Table 4), demonstrated significant improvements in robustness in cross-domain results. Moreover, the TIR method, by necessitating the use of color information in text to restore full-color images from limited grayscale patches, underscores the importance of color information in text, enhancing robustness more effectively compared to the IRR method. Regarding the loss  $\mathcal{L}_{cmt}$ , which mainly enhances the ability to discern fine differences, it was ineffective in cross-domain tests for the RSTPReid dataset, which has only 200 identities. However, for

Text	Image	Similarity			
		Baseline	IRRA	SEN	
① This person has <b>short hair</b> . She has on a <b>black skirt</b> and a <b>white top</b> . She is carrying a <b>black bag</b> on her left shoulder.		①	0.353	0.389	0.401
② She, with <b>short hair</b> , and wearing a <b>white top</b> and a <b>black skirt</b> , has her left shoulder draped with a <b>black bag</b> .		②	0.423	0.403	0.409
③ This female, in a <b>white top</b> and <b>black skirt</b> , with <b>short hair</b> , supports a <b>black bag</b> on her left shoulder.		③	0.329	0.348	0.371

Figure 8: Variations in cosine similarity for sentences with the same meaning but different expressions under various methods. The figure displays three sets of image-text pairs, detailing the specific content of each pair. On the right, “Similarity” denotes the cosine similarity scores calculated using different methods, ranging from -1 to 1.

the CUHK-PEDES and ICFG-PEDES datasets with 1,000 identities each, where subtle differences are more likely to occur, applying this method resulted in performance improvements.

In summary, by enhancing key attributes in sentences, our method mitigates the issue of differing language styles across datasets, ensuring the method’s effectiveness while maintaining its robustness.

### 5.3. Limitations of Existing Methods

While text-to-image person retrieval has seen significant progress with many methods achieving excellent results on relevant datasets, cross-domain testing has revealed a common issue with language style variation that affects the applicability of existing methods in real-world scenarios. Specifically, even if multiple sentences convey the same meaning, variations in their expression can lead to discrepancies in image-text matching outcomes (see Figure 8). This results in sentences that more closely align with the overall

style of the training set sentences achieving higher matching similarity. However, our approach has only mitigated this issue and has not fully resolved it.

## 6. Conclusion

Aiming to alleviate existing challenges in text-to-image person retrieval, we propose a novel framework named SEN. Significant performance improvements have been achieved through the introduction of novel methods such as the TIR auxiliary task and the CMT loss. Specifically, the TIR auxiliary task aims to recover missing image patches and establish implicit correspondences between phrases and image patches. Additionally, the CMT loss focuses on handling challenging samples, enhancing the model’s ability to differentiate minor differences. Furthermore, an pruning-based text data augmentation method is proposed to facilitate the recognition of key components within sentences. As a result, the correspondences between visual and textual entities are effectively strengthened, and the alignment of global features is improved. The performance on three popular benchmark datasets demonstrates the effectiveness of the proposed SEN framework. The feasibility and scalability of the CLIP model with other auxiliary task supervision will be further explored in the future work.

### Declaration of competing interest

The authors declare that they have no known competing financial interests or personal relationships that could have appeared to influence the work reported in this paper.

## Acknowledgment

This work was supported by the Key R&D Program of Yunnan Province (202102AE09001902-2).

## References

- [1] Stanislaw Antol, Aishwarya Agrawal, Jiasen Lu, Margaret Mitchell, Dhruv Batra, C Lawrence Zitnick, and Devi Parikh. Vqa: Visual question answering. In *Proceedings of the IEEE international conference on computer vision*, pages 2425–2433, 2015.
- [2] Steven Bird, Edward Loper, and Ewan Klein. Nltk: The natural language toolkit. <https://www.nltk.org>, 2009. Accessed: [2023.07].
- [3] Mathilde Caron, Hugo Touvron, Ishan Misra, Hervé Jégou, Julien Mairal, Piotr Bojanowski, and Armand Joulin. Emerging properties in self-supervised vision transformers. In *Proceedings of the IEEE/CVF international conference on computer vision*, pages 9650–9660, 2021.
- [4] Soravit Changpinyo, Piyush Sharma, Nan Ding, and Radu Soricut. Conceptual 12m: Pushing web-scale image-text pre-training to recognize long-tail visual concepts. In *Proceedings of the IEEE/CVF Conference on Computer Vision and Pattern Recognition*, pages 3558–3568, 2021.
- [5] Tianlang Chen, Chenliang Xu, and Jiebo Luo. Improving text-based person search by spatial matching and adaptive threshold. In *2018 IEEE Winter Conference on Applications of Computer Vision (WACV)*, pages 1879–1887. IEEE, 2018.

- [6] Xi Chen, Xiao Wang, Soravit Changpinyo, AJ Piergiovanni, Piotr Padlewski, Daniel Salz, Sebastian Goodman, Adam Grycner, Basil Mustafa, Lucas Beyer, et al. Pali: A jointly-scaled multilingual language-image model. *arXiv preprint arXiv:2209.06794*, 2022.
- [7] Xinlei Chen, Hao Fang, Tsung-Yi Lin, Ramakrishna Vedantam, Saurabh Gupta, Piotr Dollár, and C Lawrence Zitnick. Microsoft coco captions: Data collection and evaluation server. *arXiv preprint arXiv:1504.00325*, 2015.
- [8] Xinlei Chen, Haoqi Fan, Ross Girshick, and Kaiming He. Improved baselines with momentum contrastive learning. *arXiv preprint arXiv:2003.04297*, 2020.
- [9] Yen-Chun Chen, Linjie Li, Licheng Yu, Ahmed El Kholy, Faisal Ahmed, Zhe Gan, Yu Cheng, and Jingjing Liu. Uniter: Universal image-text representation learning. In *European conference on computer vision*, pages 104–120. Springer, 2020.
- [10] Yuhao Chen, Guoqing Zhang, Yujiang Lu, Zhenxing Wang, and Yuhui Zheng. Tipcb: A simple but effective part-based convolutional baseline for text-based person search. *Neurocomputing*, 494:171–181, 2022.
- [11] Wenliang Dai, Junnan Li, Dongxu Li, Anthony Meng Huat Tiong, Junqi Zhao, Weisheng Wang, Boyang Li, Pascale Fung, and Steven Hoi. Instructblip: Towards general-purpose vision-language models with instruction tuning, 2023.
- [12] Jacob Devlin, Ming-Wei Chang, Kenton Lee, and Kristina Toutanova. Bert: Pre-training of deep bidirectional transformers for language understanding. *arXiv preprint arXiv:1810.04805*, 2018.
- [13] Zefeng Ding, Changxing Ding, Zhiyin Shao, and Dacheng Tao. Semantically

self-aligned network for text-to-image part-aware person re-identification. *arXiv preprint arXiv:2107.12666*, 2021.

- [14] Alexey Dosovitskiy, Lucas Beyer, Alexander Kolesnikov, Dirk Weissenborn, Xiaohua Zhai, Thomas Unterthiner, Mostafa Dehghani, Matthias Minderer, Georg Heigold, Sylvain Gelly, et al. An image is worth 16x16 words: Transformers for image recognition at scale. *arXiv preprint arXiv:2010.11929*, 2020.
- [15] Zi-Yi Dou, Yichong Xu, Zhe Gan, Jianfeng Wang, Shuohang Wang, Lijuan Wang, Chenguang Zhu, Pengchuan Zhang, Lu Yuan, Nanyun Peng, et al. An empirical study of training end-to-end vision-and-language transformers. In *Proceedings of the IEEE/CVF Conference on Computer Vision and Pattern Recognition*, pages 18166–18176, 2022.
- [16] Ammarah Farooq, Muhammad Awais, Josef Kittler, and Syed Safwan Khalid. Axm-net: Implicit cross-modal feature alignment for person re-identification. In *Proceedings of the AAAI Conference on Artificial Intelligence*, volume 36, pages 4477–4485, 2022.
- [17] Chenyang Gao, Guanyu Cai, Xinyang Jiang, Feng Zheng, Jun Zhang, Yifei Gong, Pai Peng, Xiaowei Guo, and Xing Sun. Contextual non-local alignment over full-scale representation for text-based person search. *arXiv preprint arXiv:2101.03036*, 2021.
- [18] Alex Graves and Alex Graves. Long short-term memory. *Supervised sequence labelling with recurrent neural networks*, pages 37–45, 2012.
- [19] Xiao Han, Sen He, Li Zhang, and Tao Xiang. Text-based person search with limited data. *arXiv preprint arXiv:2110.10807*, 2021.

- [20] Kaiming He, Xiangyu Zhang, Shaoqing Ren, and Jian Sun. Deep residual learning for image recognition. In *Proceedings of the IEEE conference on computer vision and pattern recognition*, pages 770–778, 2016.
- [21] Kaiming He, Haoqi Fan, Yuxin Wu, Saining Xie, and Ross Girshick. Momentum contrast for unsupervised visual representation learning. In *Proceedings of the IEEE/CVF conference on computer vision and pattern recognition*, pages 9729–9738, 2020.
- [22] Kaiming He, Xinlei Chen, Saining Xie, Yanghao Li, Piotr Dollár, and Ross Girshick. Masked autoencoders are scalable vision learners. In *Proceedings of the IEEE/CVF conference on computer vision and pattern recognition*, pages 16000–16009, 2022.
- [23] Chao Jia, Yinfei Yang, Ye Xia, Yi-Ting Chen, Zarana Parekh, Hieu Pham, Quoc Le, Yun-Hsuan Sung, Zhen Li, and Tom Duerig. Scaling up visual and vision-language representation learning with noisy text supervision. In *International conference on machine learning*, pages 4904–4916. PMLR, 2021.
- [24] Ding Jiang and Mang Ye. Cross-modal implicit relation reasoning and aligning for text-to-image person retrieval. In *Proceedings of the IEEE/CVF Conference on Computer Vision and Pattern Recognition*, pages 2787–2797, 2023.
- [25] Ya Jing, Chenyang Si, Junbo Wang, Wei Wang, Liang Wang, and Tieniu Tan. Pose-guided multi-granularity attention network for text-based person search. In *Proceedings of the AAAI Conference on Artificial Intelligence*, volume 34, pages 11189–11196, 2020.
- [26] Wonjae Kim, Bokyung Son, and Ildoo Kim. Vilt: Vision-and-language trans-

former without convolution or region supervision. In *International Conference on Machine Learning*, pages 5583–5594. PMLR, 2021.

[27] DiederikP. Kingma and Jimmy Ba. Adam: A method for stochastic optimization. *arXiv: Learning, arXiv: Learning*, Dec 2014.

[28] Ryan Kiros, Ruslan Salakhutdinov, and Richard S Zemel. Unifying visual-semantic embeddings with multimodal neural language models. *arXiv preprint arXiv:1411.2539*, 2014.

[29] Ranjay Krishna, Yuke Zhu, Oliver Groth, Justin Johnson, Kenji Hata, Joshua Kravitz, Stephanie Chen, Yannis Kalantidis, Li-Jia Li, David A Shamma, et al. Visual genome: Connecting language and vision using crowdsourced dense image annotations. *International journal of computer vision*, 123:32–73, 2017.

[30] Jie Lei, Xinlei Chen, Ning Zhang, Mengjiao Wang, Mohit Bansal, Tamara L Berg, and Licheng Yu. Loopitr: Combining dual and cross encoder architectures for image-text retrieval. *arXiv preprint arXiv:2203.05465*, 2022.

[31] Junnan Li, Ramprasaath Selvaraju, Akhilesh Gotmare, Shafiq Joty, Caiming Xiong, and Steven Chu Hong Hoi. Align before fuse: Vision and language representation learning with momentum distillation. *Advances in neural information processing systems*, 34:9694–9705, 2021.

[32] Junnan Li, Dongxu Li, Caiming Xiong, and Steven Hoi. Blip: Bootstrapping language-image pre-training for unified vision-language understanding and generation. In *International Conference on Machine Learning*, pages 12888–12900. PMLR, 2022.

- [33] Junnan Li, Dongxu Li, Silvio Savarese, and Steven Hoi. Blip-2: Bootstrapping language-image pre-training with frozen image encoders and large language models. *arXiv preprint arXiv:2301.12597*, 2023.
- [34] Shiping Li, Min Cao, and Min Zhang. Learning semantic-aligned feature representation for text-based person search. In *ICASSP 2022-2022 IEEE International Conference on Acoustics, Speech and Signal Processing (ICASSP)*, pages 2724–2728. IEEE, 2022.
- [35] Shuang Li, Tong Xiao, Hongsheng Li, Wei Yang, and Xiaogang Wang. Identity-aware textual-visual matching with latent co-attention. In *Proceedings of the IEEE International Conference on Computer Vision*, pages 1890–1899, 2017.
- [36] Shuang Li, Tong Xiao, Hongsheng Li, Bolei Zhou, Dayu Yue, and Xiaogang Wang. Person search with natural language description. In *Proceedings of the IEEE conference on computer vision and pattern recognition*, pages 1970–1979, 2017.
- [37] Zhaoshuo Liu, Chaolu Feng, Shuaizheng Chen, and Jun Hu. Knowledge-preserving continual person re-identification using graph attention network. *Neural Networks*, 161:105–115, 2023. ISSN 0893-6080. doi: <https://doi.org/10.1016/j.neunet.2023.01.033>. URL <https://www.sciencedirect.com/science/article/pii/S089360802300045X>.
- [38] Yiwei Ma, Xiaoshuai Sun, Jiayi Ji, Guannan Jiang, Weilin Zhuang, and Rongrong Ji. Beat: Bi-directional one-to-many embedding alignment for text-based person retrieval. New York, NY, USA, 2023. Association for Computing Machinery. ISBN 9798400701085. doi: 10.1145/3581783.3611768. URL <https://doi.org/10.1145/3581783.3611768>.

- [39] Antoine Miech, Jean-Baptiste Alayrac, Ivan Laptev, Josef Sivic, and Andrew Zisserman. Thinking fast and slow: Efficient text-to-visual retrieval with transformers. In *Proceedings of the IEEE/CVF Conference on Computer Vision and Pattern Recognition*, pages 9826–9836, 2021.
- [40] Enhao Ning, Yangfan Wang, Changshuo Wang, Huang Zhang, and Xin Ning. Enhancement, integration, expansion: Activating representation of detailed features for occluded person re-identification. *Neural Networks*, 169:532–541, 2024. ISSN 0893-6080. doi: <https://doi.org/10.1016/j.neunet.2023.11.003>. URL <https://www.sciencedirect.com/science/article/pii/S0893608023006263>.
- [41] Vicente Ordonez, Girish Kulkarni, and Tamara Berg. Im2text: Describing images using 1 million captioned photographs. *Advances in neural information processing systems*, 24, 2011.
- [42] Alec Radford, Jong Wook Kim, Chris Hallacy, Aditya Ramesh, Gabriel Goh, Sandhini Agarwal, Girish Sastry, Amanda Askell, Pamela Mishkin, Jack Clark, et al. Learning transferable visual models from natural language supervision. In *International conference on machine learning*, pages 8748–8763. PMLR, 2021.
- [43] Nikolaos Sarafianos, Xiang Xu, and Ioannis A Kakadiaris. Adversarial representation learning for text-to-image matching. In *Proceedings of the IEEE/CVF international conference on computer vision*, pages 5814–5824, 2019.
- [44] Christoph Schuhmann, Richard Vencu, Romain Beaumont, Robert Kaczmarczyk, Clayton Mullis, Aarush Katta, Theo Coombes, Jenia Jitsev, and Aran

Komatsuzaki. Laion-400m: Open dataset of clip-filtered 400 million image-text pairs. *arXiv preprint arXiv:2111.02114*, 2021.

[45] Rico Sennrich, Barry Haddow, and Alexandra Birch. Neural machine translation of rare words with subword units. *arXiv preprint arXiv:1508.07909*, 2015.

[46] Zhiyin Shao, Xinyu Zhang, Meng Fang, Zhifeng Lin, Jian Wang, and Changxing Ding. Learning granularity-unified representations for text-to-image person re-identification. In *Proceedings of the 30th ACM International Conference on Multimedia*, pages 5566–5574, 2022.

[47] Zhiyin Shao, Xinyu Zhang, Changxing Ding, Jian Wang, and Jingdong Wang. Unified pre-training with pseudo texts for text-to-image person re-identification. In *Proceedings of the IEEE/CVF International Conference on Computer Vision*, pages 11174–11184, 2023.

[48] Fei Shen, Xiangbo Shu, Xiaoyu Du, and Jinhui Tang. Pedestrian-specific bipartite-aware similarity learning for text-based person retrieval. New York, NY, USA, 2023. Association for Computing Machinery. ISBN 9798400701085. doi: 10.1145/3581783.3612009. URL <https://doi.org/10.1145/3581783.3612009>.

[49] Xiujun Shu, Wei Wen, Haoqian Wu, Keyu Chen, Yiran Song, Ruizhi Qiao, Bo Ren, and Xiao Wang. See finer, see more: Implicit modality alignment for text-based person retrieval. In *European Conference on Computer Vision*, pages 624–641. Springer, 2022.

[50] Karen Simonyan and Andrew Zisserman. Very deep convolutional networks for large-scale image recognition. *arXiv preprint arXiv:1409.1556*, 2014.

- [51] Weijie Su, Xizhou Zhu, Yue Cao, Bin Li, Lewei Lu, Furu Wei, and Jifeng Dai. Vl-bert: Pre-training of generic visual-linguistic representations. *arXiv preprint arXiv:1908.08530*, 2019.
- [52] Siqi Sun, Yen-Chun Chen, Linjie Li, Shuohang Wang, Yuwei Fang, and Jingjing Liu. Lightningdot: Pre-training visual-semantic embeddings for real-time image-text retrieval. In *Proceedings of the 2021 Conference of the North American Chapter of the Association for Computational Linguistics: Human Language Technologies*, pages 982–997, 2021.
- [53] Ashish Vaswani, Noam Shazeer, Niki Parmar, Jakob Uszkoreit, Llion Jones, Aidan N Gomez, Łukasz Kaiser, and Illia Polosukhin. Attention is all you need. *Advances in neural information processing systems*, 30, 2017.
- [54] Zhe Wang, Zhiyuan Fang, Jun Wang, and Yezhou Yang. Vitaa: Visual-textual attributes alignment in person search by natural language. In *Computer Vision–ECCV 2020: 16th European Conference, Glasgow, UK, August 23–28, 2020, Proceedings, Part XII 16*, pages 402–420. Springer, 2020.
- [55] Zhengyang Wang, Xiufen Ye, Xue Shang, Shuzhi Sam Ge, and Shuxiang Guo. Person re-identification method with mahalanobis trm triplet on multi-branch network. *Applied Intelligence*, 2023. doi: 10.1007/s10489-023-05039-9. URL <https://doi.org/10.1007/s10489-023-05039-9>.
- [56] Zijie Wang, Aichun Zhu, Jingyi Xue, Xili Wan, Chao Liu, Tian Wang, and Yifeng Li. Caibc: Capturing all-round information beyond color for text-based person retrieval. In *Proceedings of the 30th ACM International Conference on Multimedia*, pages 5314–5322, 2022.
- [57] Zijie Wang, Aichun Zhu, Jingyi Xue, Xili Wan, Chao Liu, Tian Wang, and

Yifeng Li. Look before you leap: Improving text-based person retrieval by learning a consistent cross-modal common manifold. In *Proceedings of the 30th ACM International Conference on Multimedia*, pages 1984–1992, 2022.

[58] Hefeng Wu, Weifeng Chen, Zhibin Liu, Tianshui Chen, Zhiguang Chen, and Liang Lin. Contrastive transformer learning with proximity data generation for text-based person search. *IEEE Transactions on Circuits and Systems for Video Technology*, pages 1–1, 2023. doi: 10.1109/TCSVT.2023.3329220.

[59] Yushuang Wu, Zizheng Yan, Xiaoguang Han, Guanbin Li, Changqing Zou, and Shuguang Cui. Lapscore: language-guided person search via color reasoning. In *Proceedings of the IEEE/CVF International Conference on Computer Vision*, pages 1624–1633, 2021.

[60] Shuanglin Yan, Neng Dong, Liyan Zhang, and Jinhui Tang. Clip-driven fine-grained text-image person re-identification. *arXiv preprint arXiv:2210.10276*, 2022.

[61] Shuanglin Yan, Hao Tang, Liyan Zhang, and Jinhui Tang. Image-specific information suppression and implicit local alignment for text-based person search. *arXiv preprint arXiv:2208.14365*, 2022.

[62] Mang Ye, Jianbing Shen, Gaojie Lin, Tao Xiang, Ling Shao, and Steven C. H. Hoi. Deep learning for person re-identification: A survey and outlook. *IEEE Transactions on Pattern Analysis and Machine Intelligence*, page 2872–2893, Jun 2022. doi: 10.1109/tpami.2021.3054775. URL <http://dx.doi.org/10.1109/tpami.2021.3054775>.

[63] Jiahui Yu, Zirui Wang, Vijay Vasudevan, Legg Yeung, Mojtaba Seyedhosseini,

and Yonghui Wu. Coca: Contrastive captioners are image-text foundation models. *arXiv preprint arXiv:2205.01917*, 2022.

[64] Ying Zhang and Huchuan Lu. Deep cross-modal projection learning for image-text matching. In *Proceedings of the European conference on computer vision (ECCV)*, pages 686–701, 2018.

[65] Zhedong Zheng, Liang Zheng, Michael Garrett, Yi Yang, Mingliang Xu, and Yi-Dong Shen. Dual-path convolutional image-text embeddings with instance loss. *ACM Transactions on Multimedia Computing, Communications, and Applications (TOMM)*, 16(2):1–23, 2020.

[66] Aichun Zhu, Zijie Wang, Yifeng Li, Xili Wan, Jing Jin, Tian Wang, Fangqiang Hu, and Gang Hua. Dssl: Deep surroundings-person separation learning for text-based person retrieval. In *Proceedings of the 29th ACM International Conference on Multimedia*, pages 209–217, 2021.